

Threshold current reduction in spin-polarized lasers: Role of strain and valence-band mixing

Michael Holub and Berend T. Jonker*

Naval Research Laboratory, Washington, DC 20375, USA

(Received 7 January 2011; published 21 March 2011)

We show that valence-band mixing (VBM) plays a dominant role in determining the current threshold I_{th} of spin-pumped lasers. The degree of VBM is controlled by tuning the strain through the selection of alloy composition and layer structure. In a well-designed $\text{In}_x\text{Ga}_{1-x}\text{As}$ structure, VBM can lead to a nearly a fourfold decrease in I_{th} . However, it can also lead to a 25-fold increase for a different composition, in marked contrast to common expectations. In certain cases, larger threshold reductions are achieved for smaller injected spin polarization, a counterintuitive result.

DOI: [10.1103/PhysRevB.83.125309](https://doi.org/10.1103/PhysRevB.83.125309)

PACS number(s): 72.25.Hg, 42.55.Px, 85.70.Sq, 85.75.-d

I. INTRODUCTION

Utilization of the electron's spin offers new performance and functionality in semiconductor device structures.¹⁻³ Seminal examples include proposals for spin-polarized field-effect transistors,⁴ spin-pumped solid-state lasers,⁵ and spin-transport-based logic.⁶ Spin-polarized lasers have attracted interest recently since they promise certain advantages over conventional charge-based lasers, including reduced threshold currents,^{5,7,8} spin-based laser modulation,⁹ and polarization control.¹⁰

Initial treatments of laser threshold current reduction due to spin-polarized carrier injection predicted a twofold reduction based on qualitative arguments,⁵ and emphasized the importance of the spin polarization of the injected current. Several groups have subsequently investigated spin-polarized lasers theoretically with the aim of quantifying the maximum attainable threshold reduction. However, these estimates were obtained from either linear gain^{5,11,12} or parabolic band¹¹ models that neglected strain and band mixing, and instead treat two circularly polarized modes coupled only through spin relaxation. Since the operation of spin lasers depends critically on the polarization dependence of optical gain, it is necessary to account for valence-band mixing (VBM), which is directly related to strain in the layer, to properly model the laser quantum-well (QW) gain spectra and laser threshold current. We find that strain and/or VBM plays a dominant role, and is as important to consider as spin injection efficiency.

VBM refers to the coupling between the heavy-hole (HH), light-hole (LH), and split-off (SO) VB states due to the spin-orbit interaction, resulting in deviations from parabolic behavior. It is exhibited by virtually every semiconductor, and therefore is of broad relevance, particularly for phenomena explicitly involving hole states such as interband radiative recombination.

Here we show by detailed calculation that strain, introduced and controlled by the selection of alloy composition and layer structure, plays a dominant role in determining the lasing threshold for spin-pumped $\text{In}_x\text{Ga}_{1-x}\text{As}$ QW vertical-cavity surface-emitting lasers (VCSELs). Strain controls the degree of VBM, exhibited in varying degrees by every semiconductor, which we show has a significant impact on the spin-pumped lasing threshold. The sign and magnitude of the strain in the active lasing layer is determined by both the QW alloy composition, x , and the selection of the cladding layer (the

barrier material used for electron confinement)—these are the basic parameters of band-gap engineering. In a well-designed structure, VBM can lead to a nearly fourfold decrease in the spin-polarized threshold current. However, it can also lead to a 25-fold increase in the threshold current for a different $\text{In}_x\text{Ga}_{1-x}\text{As}$ composition, even for the case of perfect spin injection, underscoring the importance of this contribution. In certain cases, we find that larger threshold reductions are achieved for *lower* injected spin polarization, a surprising result. The largest threshold reductions are achieved using compressively strained wells in which the hole bands are well separated, minimizing VBM. Our results provide new insight into strain and/or VB effects in spin-based optical devices, and provide clear guidelines for the realization of significant threshold current reduction in spin-pumped lasers.

II. MODEL AND METHODS

Since our approach to calculating the optical gain for a QW laser has been covered extensively in the literature,^{13,14} we will discuss in detail only the modifications necessary to treat the effects of carrier spin polarization on the laser operation. The 6×6 Luttinger-Kohn Hamiltonian including biaxial strain effects is used to determine the energy dispersion of the valence subbands.¹⁴⁻¹⁶ This form of the Hamiltonian and associated basis functions are written under the assumption of spins polarized along the growth direction and for (001)-oriented substrates. Calculations performed here are thus strictly applicable to QW VCSELs only (we note that a threshold reduction is not expected for edge-emitting QW lasers since pure HH states couple to in-plane polarized light). The valence subband dispersion thus calculated for the canonical $\text{Al}_{0.2}\text{Ga}_{0.8}\text{As}/8 \text{ nm GaAs}$ QW is shown in Fig. 1, illustrating the significant deviation from parabolic behavior exhibited even in this simple system. These results agree well with those reported previously,^{13,17,18} confirming our calculational approach.

The conduction-band energy dispersion and wave functions are obtained by solving the single-band effective-mass equation using the finite difference method. Next, the optical gain at photon energy E is calculated using the following expression:

$$g(E) = \frac{\pi e^2 \hbar}{m_0^2 \epsilon_0 n_r c E} \sum_n \sum_m \iint \frac{|\hat{e} \cdot M_{mn}|^2}{4\pi L_z} (f_{c,n} - f_{v,m}) \times L[E_{n,m}(k_{\parallel})] dk_x dk_y, \quad (1)$$

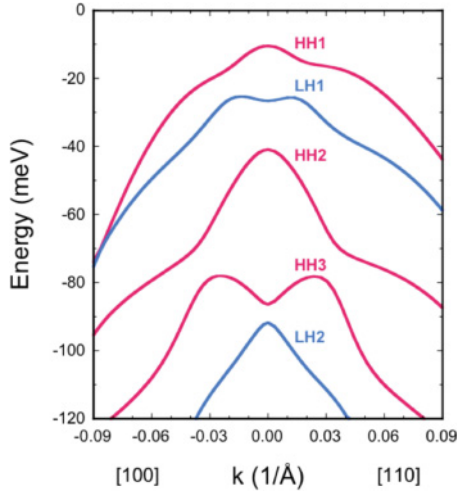


FIG. 1. (Color online) Valence subband dispersion for an $\text{Al}_{0.2}\text{Ga}_{0.8}\text{As}/8$ nm GaAs QW, illustrating the pronounced deviations from parabolic behavior due to spin-orbit-induced band mixing.

where e is the free-electron charge, \hbar is the reduced Planck constant, m_0 is the free-electron mass, ϵ_0 is the permittivity of free space, n_r is the refractive index, c is the velocity of light, and L_z is the QW thickness. The Fermi-Dirac distribution functions for the n th conduction subband and m th valence subband are given by $f_{c,n}$ and $f_{v,m}$, respectively, and the summations are performed over both spin subbands. The spin-up and spin-down electron quasi-Fermi levels are allowed to vary so as to maintain a chosen steady-state electron-spin polarization, P_e , for all carrier injection levels. We assume rapid hole spin relaxation such that the VB quasi-Fermi levels for both hole spin subbands are always identical. We consider only the case of an undoped QW, and further assume overall charge neutrality holds. The gain spectrum is convolved with a non-Markovian line-shape broadening function, $L[E_{n,m}(k_{\parallel})]$, to account for intraband relaxation processes.¹⁹

The polarization dependence of the optical gain is contained within the optical transition matrix element, which is given by

$$\hat{e} \cdot M_{nm} = \sum_{v=1}^6 \langle \varphi_{c,n} | \varphi_{v,m} \rangle \langle u_c | \hat{e} \cdot \hat{p} | u_v \rangle, \quad (2)$$

where $\varphi_{c,n}$ and $\varphi_{v,m}$ are the electron and hole envelope eigenfunctions, $\langle u_c | \hat{e} \cdot \hat{p} | u_v \rangle$ is the momentum matrix element between the conduction and valence states, and \hat{e} is a unit vector along the polarization direction of the optical field. We consider three orthogonal linearly polarized modes ($\hat{e} = \hat{x}$, \hat{y} , or \hat{z}) as well as right-circularly polarized (RCP) and left-circularly polarized (LCP) modes for which $\hat{e} = \frac{1}{\sqrt{2}}(\hat{x} + i\hat{y})$ and $\hat{e} = \frac{1}{\sqrt{2}}(\hat{x} - i\hat{y})$, respectively. Within the angular momentum convention, the band-edge optical selection rules dictate that recombination of spin-up electrons and heavy holes results in the emission of a LCP photon and recombination of spin-down electrons and heavy holes results in the emission of a RCP photon.²⁰

An expression similar to Eq. (1) may be used to calculate the spontaneous emission rate where the $(f_{c,n} - f_{v,m})$ term is replaced by $f_{c,n}(1 - f_{v,m})$ and the prefactor is multiplied by $n_r^2 E^2 / \pi^2 \hbar^3 c^2$. The total spontaneous emission rate per unit

volume, R_{sp} , is obtained from the average of the three linear polarizations, integrated over the entire emission spectrum. The radiative current density is then defined by $J_{\text{rad}} = eL_z R_{\text{sp}}$, and may be used to estimate the injection current density necessary to reach threshold in the absence of nonradiative recombination and leakage current. We note that this value of the radiative current density is independent of the chosen line-shape broadening function.

III. RESULTS AND DISCUSSION

To illustrate the impact of VBM on spin-polarized lasers, we consider two technologically important material systems: an $\text{Al}_{0.2}\text{Ga}_{0.8}\text{As}/8$ nm $\text{In}_x\text{Ga}_{1-x}\text{As}$ QW ($0 \leq x \leq 0.2$) and an $\text{In}_{0.83}\text{Ga}_{0.17}\text{As}_{0.37}\text{P}_{0.63}/6$ nm $\text{In}_x\text{Ga}_{1-x}\text{As}$ QW ($0.4 \leq x \leq 0.75$), corresponding to operating wavelength ranges of $0.85\text{--}0.98 \mu\text{m}$ and $1.35\text{--}1.8 \mu\text{m}$, respectively. The composition of the quaternary is chosen to ensure lattice matching with InP, as well as sufficient carrier confinement over a wide range of QW compositions, to explore the effects of compressive and tensile strain on the expected threshold reduction. All band and alloy bowing parameters are obtained from Ref. 21.

We calculate the peak material gain for all optical modes as a function of injected carrier density, radiative current density, and electron-spin polarization. The gain curves for all in-plane polarized modes are identical for unpolarized electrons. Whenever a threshold current reduction is observable, the preferential injection of spin-up (spin-down) electrons results in a transparency current density reduction for the LCP (RCP) mode and an increase for the remaining optical modes. Spin-induced changes in the laser threshold, which are generally largest near transparency, can be deduced from the LCP gain curves since we consider only the case of $P_e > 0$.

Figures 2(a) and 2(b) show the threshold reduction at room temperature for a fully spin-polarized electron population ($P_e = 1$) in the two InGaAs QW systems plotted as a function of in-plane strain $\epsilon_{xx} = \epsilon_{yy} = (a_0 - a)/a$, where a and a_0 are the lattice constants of the QW and substrate, respectively. We define the threshold reduction as $R = n_{\text{th}}^k(P_e = 0)/n_{\text{th}}^k(P_e)$, where n_{th} is the carrier sheet density at threshold, and k equals 1, 2, or 3 whenever the threshold current is governed by Shockley-Read-Hall (SRH), radiative, or Auger recombination, respectively. For simplicity, we assume the recombination coefficients characterizing these processes are independent of spin polarization. Figure 2 clearly demonstrates that a sizable threshold reduction as large as 3.7 is possible for compressively strained QWs, whereas a substantial increase [fivefold to 25-fold, Fig. 2(b)] can occur for unstrained and tensile-strained QWs. The threshold increase peaks for values of tensile strain that restore the HH-LH degeneracy. Note that Fig. 2(a) predicts a large increase rather than a decrease in the threshold current for the $\text{Al}_{0.2}\text{Ga}_{0.8}\text{As}/\text{GaAs}$ QW system commonly studied.

The overall laser threshold current is determined from a combination of the plotted nonradiative and radiative recombination mechanisms. The radiative component provides the dominant contribution for all compositions of the $\text{Al}_{0.2}\text{Ga}_{0.8}\text{As}/\text{In}_x\text{Ga}_{1-x}\text{As}$ system at room temperature.¹³ In contrast, Auger recombination plays a significant role for

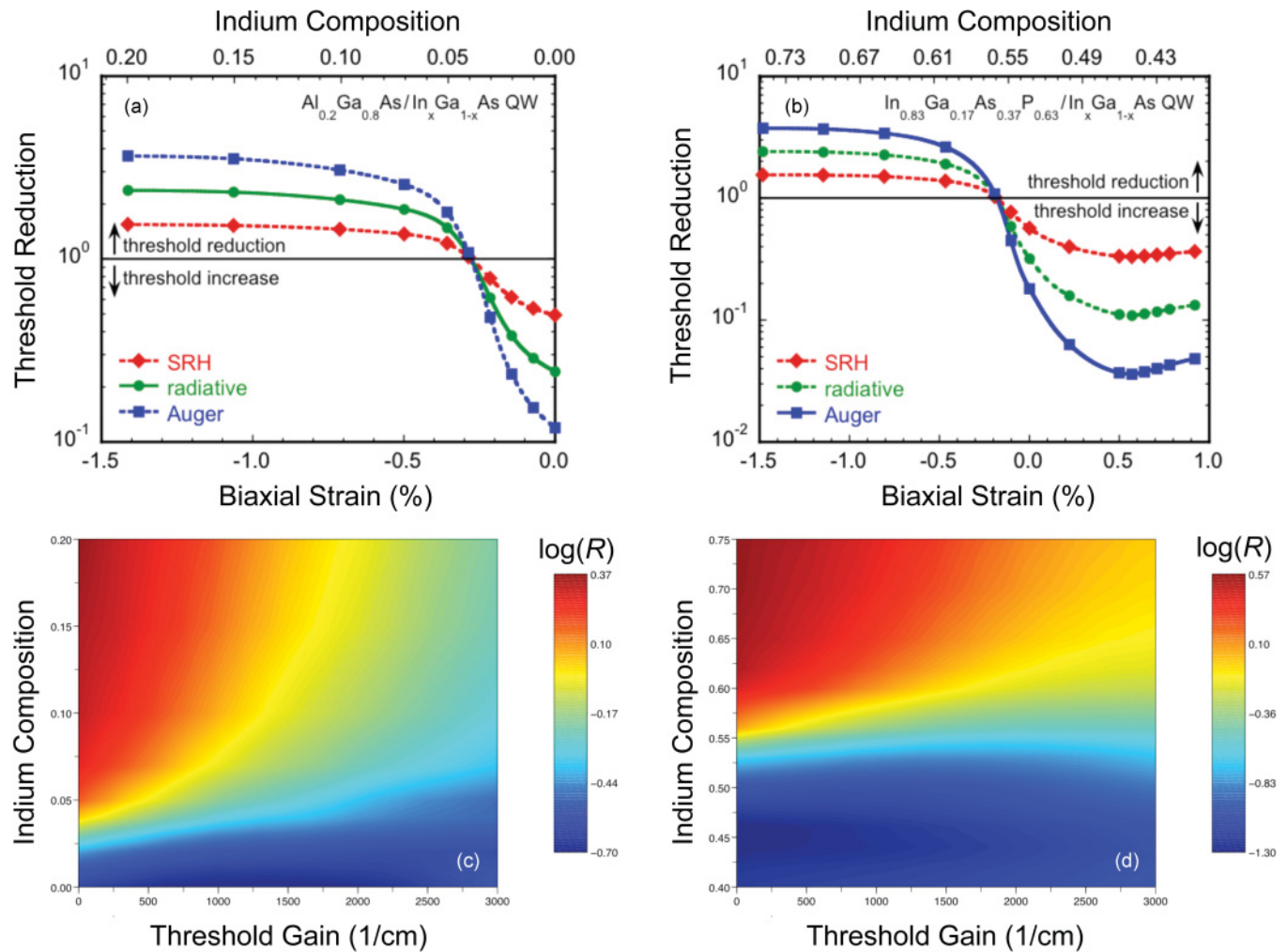


FIG. 2. (Color) Threshold reduction calculated for a fully spin-polarized electron population in an (a) Al_{0.2}Ga_{0.8}As/8 nm In_xGa_{1-x}As QW and (b) In_{0.83}Ga_{0.17}As_{0.37}P_{0.63}/6 nm In_xGa_{1-x}As QW at 300 K, assuming the threshold current is dominated by SRH, radiative, and Auger recombination. Note that values less than 1 indicate an increase in the threshold current. The lines serve as a guide to the eye, and the solid line indicates the dominant recombination mechanism expected for each material system at 300 K. Negative (positive) values of strain correspond to compressive (tensile) strain. (c) Threshold reduction (color scale) when radiative recombination dominates for an Al_{0.2}Ga_{0.8}As/8 nm In_xGa_{1-x}As QW vs indium composition and threshold gain at 300 K. (d) Threshold reduction (color scale) when Auger recombination dominates for an In_{0.83}Ga_{0.17}As_{0.37}P_{0.63}/6 nm In_xGa_{1-x}As QW vs indium composition and threshold gain at 300 K. Note that the color scale shows log₁₀(R), so that positive values correspond to a reduction and negative values correspond to an increase in threshold current.

InP-based InGaAs QW lasers, and can constitute between 60% and 90% of the total threshold current depending on the specific QW parameters.²² Contour plots of the threshold reduction as a function of In composition and threshold gain are shown for these two specific cases in Figs. 2(c) and 2(d). The color scale shows log₁₀(R), so that negative values correspond to an increase in threshold current.

The threshold reduction dependence on biaxial strain can be understood by examining the degree of VBM throughout the VB structure. Figure 3(a) shows the proportion of HH, LH, and SO components for the ground-state HH subband in the Al_{0.2}Ga_{0.8}As/In_xGa_{1-x}As QW system for select QW compositions. The states are entirely of HH character near the band edge for all indium concentrations. However, the admixture of HH and LH states increases rapidly with the in-plane wave vector. This effect is especially pronounced for the unstrained GaAs well (solid line) near $\mathbf{k} = 0.02 \text{ \AA}^{-1}$, which

coincides with the HH-LH anticrossing (Fig. 1). Compressive strain increases the HH-LH splitting and allows the HH1 subband to retain a predominately HH character over a wider range of in-plane wave vectors. The net result is a larger difference between the LCP and RCP transition strengths for any given state within the HH1 subband, as shown in Fig. 3(b).

This increasing admixture between states becomes particularly important at higher carrier densities. In spin-pumped lasers, the majority-spin electron density must increase over its value in the unpolarized case in order to compensate for the unpolarized holes due to gain saturation.¹¹ This results in lasing involving an annulus of states at a higher energy in momentum space, for which there is a greater deviation from the band-edge selection rules. While population inversion is achieved in the majority-spin conduction subband, the minority-spin subband is relatively empty, and there is a finite probability of photon reabsorption within this subband that

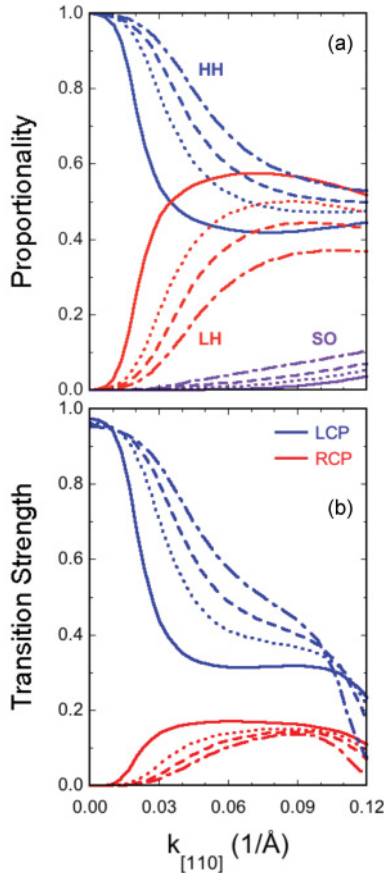


FIG. 3. (Color online) VBM and optical transition strength for circularly polarized light. (a) Proportion of the HH, LH, and SO components for the lowest HH subband in an $\text{Al}_{0.2}\text{Ga}_{0.8}\text{As}/\text{In}_x\text{Ga}_{1-x}\text{As}$ QW at 300 K. (b) Transition strength of LCP and RCP light between the lowest spin-up conduction and heavy-hole subbands at 300 K. Several indium compositions are considered: 0% (solid lines), 5% (dotted lines), 10% (dashed lines), and 20% (dashed-dotted lines).

arises from band mixing. Consequently, for sufficiently high gain levels, spin injection can result in a threshold increase for all but the most heavily compressive-strained wells, as illustrated in Figs. 2(c) and 2(d).²³

Last, we consider the threshold reduction dependence on spin polarization and temperature. Good agreement between the parabolic and band mixing models is observed only in the case of QWs with heavy compressive strain (which increases the separation of the hole bands and reduces the VBM), as shown for $\text{Al}_{0.2}\text{Ga}_{0.8}\text{As}/\text{In}_{0.2}\text{Ga}_{0.8}\text{As}$ in Fig. 4(a). A monotonic dependence on spin polarization is observed, with maximum threshold reductions of 1.54, 2.37, and 3.66 for recombination dominated by SRH, radiative, and Auger processes. Conversely, strong band mixing in QWs with little strain leads to a dramatic departure from the predictions of the parabolic band model, as shown for $\text{Al}_{0.2}\text{Ga}_{0.8}\text{As}/\text{GaAs}$ in Fig. 4(b). Surprisingly, the largest threshold reduction for an $\text{Al}_{0.2}\text{Ga}_{0.8}\text{As}/\text{GaAs}$ QW laser is obtained for moderate spin polarizations and approaches a value of $R_{\text{rad}} \approx 10\%$ at 300 K [Fig. 4(c)].

Since radiative recombination constitutes $>85\%$ of the threshold current in GaAs QW lasers at room temperature,¹⁶

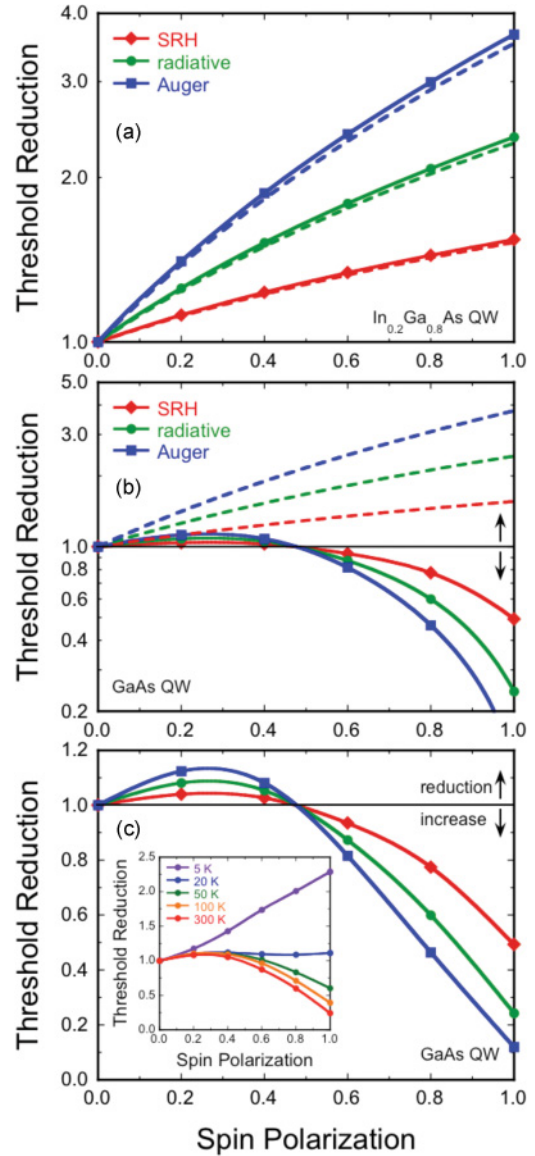


FIG. 4. (Color) Threshold reduction vs spin polarization for an (a) $\text{Al}_{0.2}\text{Ga}_{0.8}\text{As}/8\text{ nm In}_{0.2}\text{Ga}_{0.8}\text{As}$ QW and (b) $\text{Al}_{0.2}\text{Ga}_{0.8}\text{As}/8\text{ nm GaAs}$ QW at 300 K, assuming the threshold current is dominated by SRH, radiative, and Auger recombination. The solid lines serve as a guide to the eye. The dashed lines indicate the results of a parabolic model that neglects band mixing (Ref. 11). (c) Same as (b) showing a detailed dependence of the band mixing model on spin polarization. The inset shows the radiative current reduction for several temperatures.

we investigate the temperature dependence of the radiative current reduction, and the results are shown in the inset of Fig. 4(c). A monotonic dependence on spin polarization for the threshold reduction can be obtained for temperatures $<20\text{ K}$, where the transparency carrier density and thermal distribution of holes are sufficiently small to depopulate the strongly mixed hole states near the HH-LH anticrossing. It should be noted that the relevant temperature is that of the active region electron-hole plasma, which at current densities typical for cw QW laser operation can exceed the heat-sink temperature by several tens of kelvin.^{23,24} This fact would likely prevent the

observation of a strong threshold reduction in GaAs QW spin lasers even at nominally cryogenic temperatures.

IV. SUMMARY AND CONCLUSIONS

In summary, our calculations provide new insight into strain and/or VB effects in spin-based optical devices, and clear guidelines for realization of significant threshold current reduction in spin-pumped lasers. We have shown that VBM plays an important role in determining the threshold current in QW spin-pumped lasers, and must be considered as a primary design parameter in any experimental effort to realize such devices. Our results predict the range of $\text{In}_x\text{Ga}_{1-x}\text{As}$ compositions in technologically important VCSEL QW systems for which either a significant reduction or increase in threshold current should be realized. Our results are in agreement with the experimental observation of a threshold reduction of 10%–23% in GaAs/ $\text{In}_x\text{Ga}_{1-x}\text{As}$ compressively strained QW VCSELs at cryogenic temperatures,^{5,8} and only a very modest reduction of $\sim 2.5\%$ in a AlGaAs/GaAs unstrained QW

VCSEL at room temperature.⁷ Factors that should improve the chance of observing a significant threshold reduction include (a) increasing the HH-LH splitting and (b) decreasing carrier occupation in states with a large wave vector. The former may be accomplished using QWs with large compressive strain, narrow width, and large barrier height. The latter may be accomplished by reducing optical loss, increasing the number of QWs in the active region, decreasing the lattice temperature to minimize the thermal distribution of carriers, and using materials with a smaller effective mass. Secondary effects resulting from altered QW parameters, such as changes in effective mass and Auger recombination rate, must be weighed in determining whether a greater overall threshold reduction can be achieved.

ACKNOWLEDGMENTS

This work was supported by core programs in the Nanoscience Institute at NRL. M.H. gratefully acknowledges support from the National Research Council.

*Corresponding author: jonker@nrl.navy.mil

¹S. A. Wolf, D. D. Awschalom, R. A. Buhrman, J. M. Daughton, S. von Molnar, M. L. Roukes, A. Y. Chtchelkanova, and D. M. Treger, *Science* **294**, 1448 (2001).

²I. Zutic, J. Fabian, and S. Das Sarma, *Rev. Mod. Phys.* **76**, 323 (2004).

³D. D. Awschalom and M. E. Flatté, *Nat. Phys.* **3**, 153 (2007).

⁴S. Datta and B. Das, *Appl. Phys. Lett.* **56**, 665 (1990).

⁵J. Rudolph, D. Hägele, H. M. Gibbs, G. Khitrova, and M. Oestreich, *Appl. Phys. Lett.* **82**, 4516 (2003).

⁶H. Dery, P. Balal, L. Cywinski, and L. J. Sham, *Nature (London)* **447**, 573 (2007).

⁷J. Rudolph, S. Döhrmann, D. Hägele, M. Oestreich, and W. Stolz, *Appl. Phys. Lett.* **87**, 241117 (2005).

⁸M. Holub, J. Shin, D. Saha, and P. Bhattacharya, *Phys. Rev. Lett.* **98**, 146603 (2007).

⁹S. Hallstein, J. D. Berger, M. Hilpert, H. C. Schneider, W. W. Ruhle, F. Jahnke, S. W. Koch, H. M. Gibbs, G. Khitrova, and M. Oestreich, *Phys. Rev. B* **56**, R7076 (1997).

¹⁰S. Hövel, A. Bischoff, N. C. Gerhardt, M. R. Hofmann, T. Ackemann, A. Kroner, and R. Michalzik, *Appl. Phys. Lett.* **92**, 041118 (2008).

¹¹I. Vurgaftman, M. Holub, B. T. Jonker, and J. R. Meyer, *Appl. Phys. Lett.* **93**, 031102 (2008).

¹²C. Gøthgen, R. Oszwaldowski, A. Petrou, and I. Zutic, *Appl. Phys. Lett.* **93**, 042513 (2008).

¹³L. A. Coldren and S. W. Corzine, *Diode Lasers and Photonic Integrated Circuits* (Wiley, New York, 1995).

¹⁴S. L. Chuang, *Physics of Photonic Devices* (Wiley, Hoboken, 2009).

¹⁵J. M. Luttinger and W. Kohn, *Phys. Rev.* **97**, 869 (1955).

¹⁶R. People and S. K. Sputz, *Phys. Rev. B* **41**, 8431 (1990).

¹⁷A. T. Meney, B. Gonul, and E. P. O'Reilly, *Phys. Rev. B* **50**, 10893 (1994).

¹⁸M. P. Houg, Y. C. Chang, and W. I. Wang, *J. Appl. Phys.* **64**, 4609 (1988).

¹⁹S. R. Chinn, P. S. Zory, and A. R. Reisinger, *IEEE J. Quantum Electron.* **24**, 2191 (1988).

²⁰F. Meier and B. P. Zakharchenya, *Optical Orientation*, Modern Problems in Condensed Matter Science Series, Vol.8 (North-Holland, Amsterdam, 1984).

²¹I. Vurgaftman, J. R. Meyer, and L. R. Ram-Mohan, *J. Appl. Phys.* **89**, 5815 (2001).

²²M. Silver, E. P. O'Reilly, and A. R. Adams, *IEEE J. Quantum Electron.* **33**, 1557 (1997).

²³See supplemental material at [<http://link.aps.org/supplemental/10.1103/PhysRevB.83.125309>] for further discussion.

²⁴V. I. Tolstikhin and M. Willander, *IEEE J. Quantum Electron.* **31**, 814 (1995).

²⁵G. E. Shtengel, R. F. Kazarinov, G. L. Belenky, M. S. Hybertsen, and D. A. Ackerman, in *Advances in Semiconductor Lasers and Application to Optoelectronics*, edited by M. Dutta and M. A. Strosio (World Scientific, Singapore, 2000), pp. 932 and references therein.